
Seeing the Pose in the Pixels: Learning Pose-Aware Representations in Vision Transformers

Dominick Reilly
UNC Charlotte

Aman Chadha*
Stanford University, Amazon Alexa AI

Srijan Das
UNC Charlotte

dreilly1@charlotte.edu

Abstract

Human perception of surroundings is often guided by the various poses present within the environment. Many computer vision tasks, such as human action recognition and robot imitation learning, rely on pose-based entities like human skeletons or robotic arms. However, conventional Vision Transformer (ViT) models uniformly process all patches, neglecting valuable pose priors in input videos. We argue that incorporating poses into RGB data is advantageous for learning fine-grained and viewpoint-agnostic representations. Consequently, we introduce two strategies for learning pose-aware representations in ViTs. The first method, called **Pose-aware Attention Block (PAAB)**, is a plug-and-play ViT block that performs localized attention on pose regions within videos. The second method, dubbed **Pose-Aware Auxiliary Task (PAAT)**, presents an auxiliary pose prediction task optimized jointly with the primary ViT task. Although their functionalities differ, both methods succeed in learning pose-aware representations, enhancing performance in multiple diverse downstream tasks. Our experiments, conducted across seven datasets, reveal the efficacy of both pose-aware methods on three video analysis tasks, with PAAT holding a slight edge over PAAB. Both PAAT and PAAB surpass their respective backbone Transformers by up to 9.8% in *real-world action recognition* and 21.8% in *multi-view robotic video alignment*. Code is available at <https://github.com/dominickrei/PoseAwareVT>.

1 Introduction

Despite the recent advancements in AI, video understanding remains a formidable task within the field of computer vision. Transformers [67, 18, 64, 12, 73, 29], referenced in many recent studies, have proven their dominance across various domains, including vision, thanks to their effective use of self-attention and feed-forward layers. When these transformers are applied to spatio-temporal domains, video transformers [6, 3, 41, 45, 20] have demonstrated significant potential. However, one limitation is that these video transformers treat all input patches uniformly without accounting for any priors, when applying operations. This holistic approach is effective for web-sourced videos [32, 7, 60, 35], where prominent motion patterns are typically centered within the image frames. However, the effectiveness of these transformers tends to fall short when employed on daily living videos [38, 53, 15, 68, 69] containing subtle motion, non choreographed scenes and varying camera viewpoints. Understanding these videos require learning fine-grained and camera viewpoint agnostic representations.

Daily living videos often contain entities defined by their poses. However, traditional ViTs tend to overlook these pose-based entities during video processing. The effectiveness of 3D pose information is well established in video analysis [56, 42, 19, 39, 33]. Nevertheless, these pose-based methods are

*This work is unrelated to the position at Amazon.

somewhat limited in their ability to model the appearance of a scene. To address this shortcoming, some studies [5, 4, 16] have attempted to combine 3D poses with RGB. Yet, we posit that acquiring 3D poses can be challenging, especially in the absence of a depth sensor, due to the relative inaccuracy of available algorithms and their high computational costs.

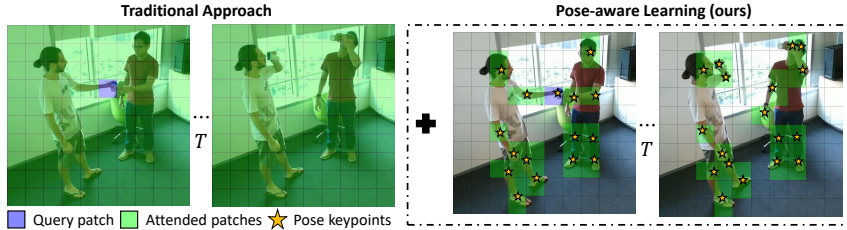


Figure 1: **The goal of our proposed framework.** Our aim is to learn pose-aware features for ViTs, while maintaining the whole-scene knowledge learned in the traditional approach to training ViTs.

Consequently, in this paper, we propose learning pose-aware video representations within ViTs by utilizing the capabilities of 2D pose keypoints (see Figure 1). These keypoints, known for their precision, can be easily extracted using readily available pose estimation algorithms [8]. To enable the learning of pose-aware representation, we propose two approaches: the first involves the formulation of a network architecture explicitly tailored for localized attention on pose patches and the second introduces an auxiliary pose prediction task that is jointly optimized with the primary task. These approaches has culminated in the introduction of two novel methods: **Pose-aware Attention Block (PAAB)** and **Pose-aware Auxiliary Task (PAAT)**. Both PAAB and PAAT can be plugged into an existing ViT, with an auxiliary loss being added for the latter. Despite their differing functionalities, both PAAB and PAAT learn to disentangle between pose and non-pose patches within a video. Our analysis leads us to the striking observation that the learned pose-aware representations are not merely a result of the pose-guided sparsity of the ViT’s attention weights, but are instead achieved through the feed-forward layers within the ViT. The efficacy of PAAB and PAAT is validated across three downstream tasks encompassing three datasets for action recognition, four for multi-view robotic video alignment, and a cross-data evaluation for video retrieval. Both PAAB and PAAT significantly outperform the baseline Transformer across all datasets, achieving state-of-the-art results relative to representative baselines.

2 Background: Attention in Video Transformers

Pose-aware representation learning is based on incorporating pose information into the training process of existing ViTs. As such, we briefly review how attention is performed in ViT’s for video data. Consider a video input of size $\tau \times H \times W \times 3$, where τ frames have a spatial resolution of $H \times W$ and three color channels. Most video transformers [50] extract disjoint patches from the video, resulting in an input sequence of ST tokens, with S being the spatial resolution and T being the temporal resolution. Each of these tokens are then projected to \mathbb{R}^D via a linear layer. Subsequently, two learnable position embeddings are added to each token to encode spatial and temporal position information, respectively. Furthermore, a class token is added to the input sequence prior to its processing by the transformer to enable the classification of the entire video. Note that this class token can be used for performing other downstream tasks as well.

Similarly to the standard transformer, the input sequence is transformed into key, query, and value matrices denoted as $\mathbf{K} \in \mathbb{R}^{ST \times D}$, $\mathbf{Q} \in \mathbb{R}^{ST \times D}$, and $\mathbf{V} \in \mathbb{R}^{ST \times D}$, respectively. Conventional self-attention [67] computes the pairwise similarities between all combinations of tokens in the input sequence. In the realm of video transformers this is known as *joint space-time attention*, as similarity is computed between all tokens, regardless of their spatial or temporal position as:

$$\alpha_{st}^{\text{joint}} = \frac{\exp(\mathbf{Q}_{st} \mathbf{K}^{\top})}{\sum_{s't'} \exp(\mathbf{Q}_{st} \mathbf{K}_{s't'}^{\top})} \quad (1)$$

where, \mathbf{Q}_{st} , $\mathbf{K}_{s't'}$ are the D -dimensional query and key vector for the token at spatial and temporal position s, t respectively. However, this approach for computing attention in video transformers is expensive due to the quadratic complexity of self-attention and the large size of video data. To

address this, factorized self-attention has been proposed in [6]. This mechanism is termed *divided space-time attention* and is achieved by applying temporal-attention followed by spatial-attention as:

$$\alpha_{st}^{\text{time}} = \frac{\exp(\mathbf{Q}_{st}\mathbf{K}_{s:}^\top)}{\sum_{t'} \exp(\mathbf{Q}_{st}\mathbf{K}_{s:t'}^\top)}; \quad \alpha_{st}^{\text{spatial}} = \frac{\exp(\mathbf{Q}_{st}\mathbf{K}_{:t}^\top)}{\sum_{s'} \exp(\mathbf{Q}_{st}\mathbf{K}_{s:t}^\top)} \quad (2)$$

where, $\mathbf{K}_{:t}$ indicates a slice of \mathbf{K} across the t^{th} frame (i.e., the keys for all spatial tokens in frame t). The remaining operations within video transformers follow the same principles as standard vision transformers [18].

3 Pose-Aware Representation Learning

This section presents our approaches to learning pose-aware representations by utilizing existing Vision Transformer (ViT) architectures for video understanding. Towards this objective, we propose two distinct approaches. The first approach entails introducing architectural changes through the incorporation of a novel PAAB that integrates knowledge of poses into the ViT representation. In contrast, the second approach involves the use of PAAT, a multi-tasking objective function to reinforce the ViT’s focus on poses, facilitating the learning of pose-aware representations.

3.1 Pose map instantiations

Due to the nature of our methods, we must have a correspondence between the video patches and the pose configurations of objects within the video. We achieve this through the construction of two pose maps: \mathcal{P}^{2D} and \mathcal{P}^{3D} , the details of which are described below.

The pose configuration of an object in a video is typically characterized by its 2D pose, which is represented by a set of 2D coordinates (known as keypoints) that provides the specific locations of relevant parts of the object. For instance, in human action videos these keypoints correspond to the locations of various human joints (hand, foot, etc) in each video frame. The localization of these keypoints can be achieved by exploiting pose estimation algorithms such as [8, 21], which are high precision algorithms and are commonly used in video analysis. After extracting these keypoints, we obtain a set \mathcal{K} that denotes the coordinates of the keypoints within each frame:

$$\mathcal{K} = \{(t, k, x, y)\} : 1 \leq t \leq \tau, 1 \leq k \leq K \quad (3)$$

where K is the number of keypoints. We then define a pose map, \mathcal{P} , of resolution $\tau \times K \times H \times W$ as:

$$\mathcal{P}_{tkxy} = \begin{cases} 1 & \text{if } (t, k, x, y) \in \mathcal{K} \\ 0 & \text{otherwise} \end{cases} \quad (4)$$

Thus, $\mathcal{P}_{tkxy} = 1$ if the k^{th} keypoint is present at the $(x, y)^{\text{th}}$ pixel in the t^{th} video frame. To align with ViT inputs, \mathcal{P} is decomposed into ST disjoint patches, transforming \mathcal{P} into a $K \times ST \times p \times p$ dimensional binary matrix, where p is the patch size. Each patch is transformed as $\mathcal{P}_i^{2D} = \text{MaxPool}(\mathcal{P}_i)$, i.e., if the patch \mathcal{P}_i contains one or more keypoints, it is set to one, else it remains zero. Thus, \mathcal{P}^{2D} is a ST dimensional binary vector indicating the video patches that contain *any* keypoints.

We also compute a 3D instantiation of the pose map, denoted as \mathcal{P}^{3D} . In contrast to \mathcal{P}^{2D} , $\mathcal{P}_{ik}^{3D} = 1$ if the k^{th} keypoint lies in the patch \mathcal{P}_i , otherwise it is zero. Thus, \mathcal{P}^{3D} is a $ST \times K$ dimensional binary vector indicating video patches that contain *a specific* keypoint.

3.2 Pose-Aware Attention Block (PAAB)

The Pose-Aware Attention Block (PAAB) is a plug-in module that can be inserted into existing ViT architectures to induce learning of pose-aware representations. When inserted into a ViT, PAAB will process tokens from the previous layer and return a set of tokens enriched with pose information, these enriched tokens can be propagated as usual through the rest of the ViT. PAAB accomplishes this through a pose-aware self-attention mechanism, restricting interactions to tokens representing human keypoints, i.e., *pose tokens*. Essentially, PAAB functions as a local attention that modulates the pose token representation based on its interaction with other pose tokens within a video. As

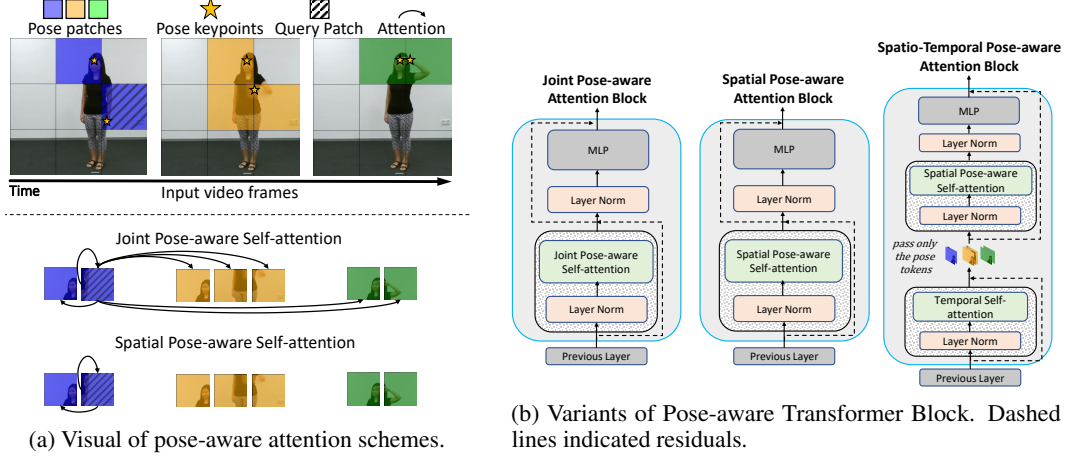


Figure 2: **Overview of Pose-Aware Attention Block.** PAAB takes tokens processed by a ViT as input and applies a pose-aware attention to them. The attention is applied jointly (over pose tokens from all frames), spatially (over pose tokens in a single frame), or spatio-temporally. In spatio-temporal attention, traditional temporal attention is applied followed by pose aware spatial attention.

shown in Figure 2b, PAAB comes in three variants, namely, joint (Joint PA-STA), spatial (PA-SA), and spatio-temporal (Factorized PA-STA) pose-aware self-attention, each differing based on how pose tokens interact with each other.

The joint variant of PAAB (see Figure 2a) extends the joint space-time attention in equation 1 by leveraging the 2D pose map \mathcal{P}^{2D} as

$$\alpha_{st}^{\text{PA-joint}} = \begin{cases} \frac{\exp(\mathbf{Q}_{st}\mathbf{K}^\top \odot \mathcal{P}^{2D})}{\sum_{s't'} \exp(\mathbf{Q}_{st}\mathbf{K}_{s't'}^\top \odot \mathcal{P}_{s't'}^{2D})} & \text{if } \mathcal{P}_{st}^{2D} = 1 \\ \mathbf{0} & \text{if } \mathcal{P}_{st}^{2D} = 0 \end{cases} \quad (5)$$

where \odot is the Hadamard product. Similarly, a spatial variant of PAAB learns attention weights $\alpha_{st}^{\text{PA-spatial}}$ for the token at (s, t) as,

$$\alpha_{st}^{\text{PA-spatial}} = \begin{cases} \frac{\exp(\mathbf{Q}_{st}\mathbf{K}_{s,t}^\top \odot \mathcal{P}_{s,t}^{2D})}{\sum_{s',t'} \exp(\mathbf{Q}_{st}\mathbf{K}_{s't'}^\top \odot \mathcal{P}_{s't'}^{2D})} & \text{if } \mathcal{P}_{st}^{2D} = 1 \\ \mathbf{0} & \text{if } \mathcal{P}_{st}^{2D} = 0 \end{cases} \quad (6)$$

Using \mathcal{P}^{2D} , the spatial attention in PAAB allows interaction amongst pose tokens in a single frame (see Figure 2a). The spatio-temporal variant of PAAB entails temporal attention α^{time} , applied to all tokens as described by equation 2. This is then followed by a pose-aware spatial attention $\alpha^{\text{PA-spatial}}$, as depicted by equation 6. Note that the aforementioned conditional pose-aware attention weights are implemented in practice through a differential approximation, whereby $\mathcal{P}^{2D} = \infty(\mathcal{P}^{2D} - 1)$ is transformed, followed by adding (instead of Hadamard product) with $\mathbf{Q}_{st}\mathbf{K}^\top$, as performed in equation 5 and 6. This equates to masking out the attention values of all non-pose tokens, similarly to how the decoder in NLP transformers masks out unseen tokens [67].

3.3 Pose-Aware Auxiliary Task (PAAT)

In contrast to PAAB, which utilizes a local attention mechanism to facilitate pose-aware representation learning, PAAT attempts at achieving the same through the introduction of an auxiliary task that is jointly optimized alongside the primary ViT task. When inserted into a ViT, PAAT's goal is to classify the specific keypoints present in each patch using the intermediate token representations obtained from the ViT layer preceding PAAT. In other words, its goal is to predict the 3D pose map \mathcal{P}^{3D} . This task can be realized as a multi-label multi-class classification problem, as each patch can contain multiple keypoints (illustrated in Figure 3a).

Given a set of tokens from the layer preceding PAAT, $\mathbf{z}_{l-1} \in \mathbb{R}^{ST \times D}$, PAAT predicts the 3D pose map introduced in section 3.1. Recall that each D -dimensional token in \mathbf{z}_{l-1} corresponds to the latent representation of a video patch from the $(l-1)^{\text{th}}$ ViT layer. As depicted in Figure 3b, PAAT is formulated as a *patch-keypoint classifier* that is composed of two linear layers defined by the weights $\mathbf{W}_1 \in \mathbb{R}^{D \times D_e}$ and $\mathbf{W}_2 \in \mathbb{R}^{D_e \times K}$, where D_e is the bottleneck dimension and $D_e \leq D$. The 3D pose map predicted by PAAT inserted at l^{th} layer of a ViT is given by:

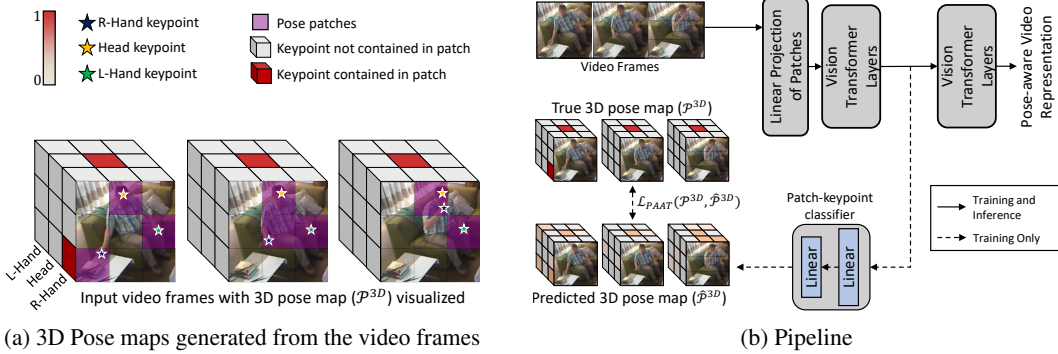


Figure 3: **Overview of Pose-Aware Auxiliary Task.** Given the 3D pose map, PAAT learns to predict the specific keypoint present within each video patch. This task is learned at train time via the patch-keypoint classifier, and can be discarded at inference time.

$$\hat{\mathcal{P}}^{3D} = \sigma((\mathbf{z}_{l-1} \mathbf{W}_1) \mathbf{W}_2) \quad (7)$$

where σ is the sigmoid activation. For brevity, we omit the bias terms. PAAT’s loss is computed as the binary cross-entropy (BCE) between \mathcal{P}^{3D} and $\hat{\mathcal{P}}^{3D}$. During training, PAAT is optimized jointly with the primary task, such as classification or video alignment, with a loss $\mathcal{L}_{primary}$. Consequently, PAAT loss, \mathcal{L}_{PAAT} , and model’s total loss, \mathcal{L}_{total} , is defined as,

$$\mathcal{L}_{PAAT} = \text{BCE}(\mathcal{P}^{3D}, \hat{\mathcal{P}}^{3D}); \quad \mathcal{L}_{total} = \lambda \mathcal{L}_{PAAT} + \mathcal{L}_{primary} \quad (8)$$

where λ is a scaling factor that controls the influence of PAAT on the model training. At training, the gradient updates with $\frac{\partial \mathbf{z}_{l-1}}{\partial \mathcal{L}_{PAAT}}$ at the $(l-1)^{th}$ layer force the ViT to learn pose-aware representations that discriminate between pose and non-pose tokens. This enables the remaining transformer layers to encode pose-aware representations. At inference, the patch-keypoint classifier is discarded and the ViT can be used with no remnants of PAAT.

4 Experiments

We evaluate the effectiveness of the proposed pose-aware learning methods on three diverse computer vision tasks: (i) action recognition, (ii) multi-view robotic video alignment, and (iii) video retrieval. We provide an experimental analysis that demonstrates the effectiveness of our methods across these diverse tasks. We also perform an extensive diagnosis on our model and discuss the intriguing properties we observe.

4.1 Datasets & Evaluation protocols

Action recognition is a popular video analysis task whose goal is to learn to predict an action label given a trimmed video. For this task we evaluate our methods on three popular Activities of Daily Living (ADL) datasets: **Toyota-Smarthome** [15] (Smarthome, SH), **NTU-RGB+D** [53] (NTU), and **Northwestern-UCLA Multiview activity 3D Dataset** [69] (NUCLA). For the Toyota-Smarthome dataset, we adhere to the cross-subject (CS) and cross-view (CV1, CV2) protocols, gauging performance using the mean class-accuracy (mCA) metric. When assessing the NTU-RGB+D dataset, we follow the cross-view-subject (CVS) protocols proposed in [66], as they better represent the cross-view challenge. As for the NUCLA dataset, we report the accuracy on cross-subject (CS), cross-view (CV3), and the average across all the cross-view protocols. For the extraction of 2D pose keypoints, we employed LCRNet [48], Randomized Decision Forest [57], and OpenPose [8] for Smarthome, NTU and NUCLA datasets respectively. Note that all our ablation studies are conducted on the action classification task.

Multi-view robotic video alignment is a task to learn a frame-to-frame mapping between video pairs acquired from different camera viewpoints. Such tasks are able to facilitate robot imitation learning from third-person viewpoints [55]. For this task we use the **Minecraft** (MC), **Pick, Can,** and **Lift** datasets. These datasets are obtained from a range of environments: Minecraft from video game whereas Pick, Can, and Lift from robotics simulators (PyBullet[14], Robomimic[44]). The pixel positions of the robotic arms, regarded as the poses, are obtained from the simulators. This task is

Table 1: **Ablations on PAAB and PAAT.** We perform ablations on the following: (a) position of PAAB and PAAT, (b) variants of PAAB, (c) number of PAABs to insert, and (d) variants of PAAT.

(a) PAAB performs best when inserted near the end of the model, PAAT performs best when inserted at the beginning. Inserting the PAAB or PAAT at multiple positions is not necessary.

| Dataset | Baseline | PAAB Position | | | | | PAAT Position | | | | |
|------------|----------|---------------|-------------|-------------|------|------|---------------|------|------|------|------|
| | | 1 | 6 | 12 | 1,6 | 1,12 | 1 | 6 | 12 | 1,6 | 1,12 |
| SH (CS) | 68.4 | 67.1 | 67.7 | 71.4 | 67.1 | 68.6 | 72.5 | 70.9 | 69.9 | 70.7 | 70.2 |
| SH (CV1) | 50.0 | 50.5 | 52.4 | 54.9 | 51.5 | 50.5 | 54.8 | 52.2 | 47.6 | 49.7 | 51.5 |
| NTU (CVS1) | 83.5 | 85.0 | 85.7 | 85.2 | 85.5 | 85.2 | 85.4 | 85.2 | 84.5 | 84.6 | 84.2 |

(b) PA-SA is sufficient despite having the least additional parameters.

| Dataset | PA-SA | Factorized PA-STA | Joint PA-STA |
|------------|-------------|-------------------|--------------|
| SH (CS) | 71.4 | 69.9 | 69.8 |
| SH (CV1) | 54.9 | 50.2 | 52.0 |
| NTU (CVS1) | 85.2 | 85.4 | 85.8 |
| NTU (CVS3) | 51.6 | 51.3 | 49.2 |

(c) Inserting 1 PAAB after layer 12 is the most consistent across datasets.

| Dataset | # PAABs at layer 12 | | | |
|------------|---------------------|------|-------|-------------|
| | 1 | 2 | 3 | 4 |
| SH (CS) | 71.4 | 67.1 | 69.0 | 66.7 |
| SH (CV1) | 54.9 | 51.3 | 51.18 | 48.4 |
| NTU (CVS1) | 85.2 | 84.7 | 85.0 | 85.6 |

(d) PAAT performs best when predicting \mathcal{P}^{3D} over \mathcal{P}^{2D}

| Dataset | Variant | Accuracy |
|------------|--------------------|-------------|
| SH (CS) | \mathcal{P}^{2D} | 71.1 |
| | \mathcal{P}^{3D} | 72.5 |
| NTU (CVS1) | \mathcal{P}^{2D} | 84.0 |
| | \mathcal{P}^{3D} | 85.4 |

evaluated by an alignment error metric introduced in [51]. Sample frames from these datasets are provided in Fig. 6.

Video Retrieval is a nearest-neighbour retrieval task performed on learned features without any further training. For evaluation, we report the Recall at k ($R@k$), meaning, if the top k nearest neighbours contains one video of the same class, the retrieval was successful.

4.2 Implementation

In our default implementations of PAAB, we use the spatial attention variant (PA-SA) inserted after the 12th layer of a backbone ViT. For PAAT, we insert it after the 1st layer of the backbone. For the implementation of PAAT, we use a bottleneck dimension (D_e) of 256 for the patch-keypoint classifier and a loss scale (λ) of 1.6. In our experiments, we use a TimeSformer [6] backbone for the task of action recognition and video retrieval, while a DeiT [64] backbone is utilized for video alignment. All other training and dataset specific details are provided in the Appendix.

4.3 Ablation studies

Where should we insert PAAB and PAAT? In Table 1a, we investigate the optimal insertion point of PAAB and PAAT. We initially examine the performance impact of incorporating a single PAAB or PAAT after specific ViT layers. Subsequently, we assess the implications of integrating multiple PAABs or PAATs at varying ViT layers. Interestingly, our findings suggest a complementary dynamic between PAAB and PAAT. PAAB exhibits superior performance when positioned closer to the ViT’s classification head, while PAAT performs better when inserted at the initial layer. This shows that the auxiliary task is beneficial for improving the primary task, namely action recognition, when operating on low-level token representations that have not yet been contextualized [1]. In contrast, attention blocks like PAAB are most effective when working with high-level token representations, which have been extensively contextualized and optimized for the primary task.

Which variant of PAAB and PAAT should be used? Here, we explore the different variants of PAAB and PAAT. Table 1b presents the classification results of different PAAB variants. These attention variants are arranged from left to right, corresponding to the number of extra parameters they introduce. Across the Smarthome and NTU datasets, PA-SA consistently exhibits superior performance, while the other two variants tend to result in a significant decrease in performance (for instance, a reduction of 2.81% on Smarthome (CS) when transitioning from PA-SA to Joint PA-STA). In general, despite having the lowest number of added parameters, PA-SA proves to be sufficient for learning pose-aware representations. In Table 1d, we analyze the implications of training PAAT with an alternate auxiliary task. This task involves predicting the presence or absence of a keypoint in each patch, rather than the specific keypoint located in each patch. Essentially, the task’s objective is to predict the 2D pose map instantiation, \mathcal{P}^{2D} . We ascertain that the patch-keypoint prediction

task (predicting \mathcal{P}^{3D}), proves more effective, underlining the significance of incorporating human anatomy knowledge into the learned video representation.

How many PAAB’s should you use? In Table 1c, we examine the optimal number of consecutive PAABs to be incorporated into the ViT. Our findings suggest that a single PAAB is sufficient, and the model’s performance tends to decline with an increased number of blocks. This outcome is attributed to the fact that incorporating additional PAABs leads to a loss of the valuable contextual information from non-pose tokens, which are often crucial for action recognition.

Table 2: Results of training our models with and without random 2D and 3D pose maps.

| Dataset | Method | Random pose map | Accuracy (%) |
|--------------|--------|-----------------|--------------|
| SH (CS) | PAAB | ✓ | 70.1 |
| | | ✗ | 71.4 |
| | PAAT | ✓ | 69.5 |
| | | ✗ | 72.5 |
| NTU60 (CVS1) | PAAB | ✓ | 85.0 |
| | | ✗ | 85.8 |
| | PAAT | ✓ | 84.8 |
| | | ✗ | 85.4 |

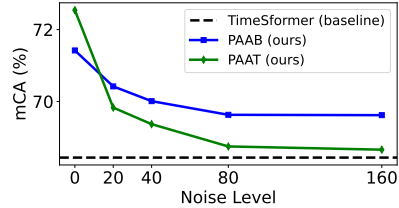


Figure 4: Model performance degrades as we lose more of the pose information.

4.4 Do poses really help?

To answer this question, we perform two experiments to evaluate the importance of poses. In our first experiment, we randomly activate values in the pose maps, \mathcal{P}^{2D} and \mathcal{P}^{3D} , irrespective of the actual presence or absence of pose keypoints in a patch. Our results, presented in Table 2, show that our methods deliver superior performance when utilizing accurate pose maps informed by pose estimation as opposed to random pose maps. In the second experiment, we introduce varying levels of noise to the pose keypoints before computing \mathcal{P}^{2D} and \mathcal{P}^{3D} . More specifically, we set a noise level $\epsilon \geq 0$ and add a randomly generated integer between 0 and ϵ to the 2D coordinates of each pose keypoint in \mathcal{K} . We then generate the pose maps as usual and train our models. The results of this experiment, conducted on the Smarthome CS protocol, are presented in Figure 4. As the reliability of the poses decreases, the accuracy of the model with PAAT quickly declines towards the baseline. On the other hand, while the accuracy of the model with PAAB also drops, it stabilizes at around 70%. These experiments show the crucial role of poses in video understanding and demonstrate the robustness of PAAB and PAAT to considerable noise in pose information.

Table 3: TimeSformer + our pose-aware methods, compared to the SOTA models on Toyota-Smarthome. Modality indicates the modalities required at inference time.

| Method | Modality | | Accuracy (%) | | |
|--------------------|----------|------|--------------|-------------|-------------|
| | RGB | Pose | CS | CV1 | CV2 |
| I3D [10] | ✓ | ✗ | 53.4 | 34.9 | 45.1 |
| VPN [16] | ✓ | 3D | 60.8 | 43.8 | 53.5 |
| AssembleNet++ [49] | ✓ | ✗ | 63.6 | - | - |
| VPN++ [17] | ✓ | 3D | 71.0 | - | 58.1 |
| MMNet [72] | ✓ | 2D | 70.1 | 37.4 | 46.6 |
| Video Swin [41] | ✓ | ✗ | 69.8 | 36.6 | 48.6 |
| MotionFormer [45] | ✓ | ✗ | 65.8 | 45.2 | 51.0 |
| TimeSformer [6] | ✓ | ✗ | 68.4 | 50.0 | 60.6 |
| PAAB (ours) | ✓ | 2D | 71.4 | 54.9 | 61.8 |
| PAAT (ours) | ✓ | ✗ | 72.5 | 54.8 | 62.2 |

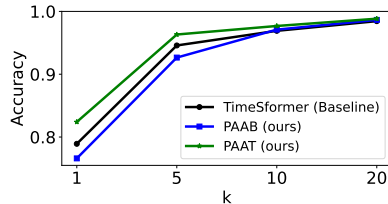


Figure 5: NTU (CS) pre-trained PAAT & PAAB (with TimeSformer backbone) for k-NN video retrieval on NUCLA. Notably, PAAT performs better at k = 1, 5, 10

4.5 Results

In this section, we present the performance of our models across three downstream tasks, and present a state-of-the-art comparison with the representative baselines.

Action recognition. We compare the performance of PAAB and PAAT to various state-of-the-art (SOTA) methods on the Smarthome, NTU, and NUCLA datasets in Table 3 and Table 4 (a-b). Our results reveal that PAAB and PAAT set a new benchmark on the Smarthome dataset which presents the challenges of real-world scenarios, including challenges in pose estimation. For a fair comparison with our models, we have primarily included models that leverage the RGB modality for the NTU

Table 4: State-of-the-art comparison on NTU-RGB+D and NUCLA.

(a) TimeSformer + our pose-aware methods on NTU. (b) TimeSformer+our pose-aware methods on NUCLA.

| Method | Modality | | Accuracy (%) | | |
|-------------------|----------|------|--------------|-------------|-------------|
| | RGB | Pose | CVS1 | CVS2 | CVS3 |
| ST-GCN[25] | ✗ | 3D | 74.8 | 59.8 | 31.4 |
| 3D ResNet-50 [30] | ✓ | ✗ | 83.9 | 67.9 | 42.9 |
| S3D [70] | ✓ | ✗ | 84.1 | 66.4 | 40.1 |
| Video Swin [41] | ✓ | ✗ | 86.9 | 72.7 | 51.4 |
| MotionFormer [45] | ✓ | ✗ | 85.3 | 72.2 | 51.3 |
| TimeSformer [6] | ✓ | ✗ | 83.5 | 72.6 | 50.3 |
| PAAB (ours) | ✓ | 2D | 85.8 | 73.1 | 51.6 |
| PAAT (ours) | ✓ | ✗ | 85.4 | 73.1 | 51.8 |

| Method | Modality | | Accuracy (%) | | |
|-------------------|----------|------|--------------|-------------|-------------|
| | RGB | Pose | CS | CV3 | Avg |
| Glimpse Cloud [5] | ✓ | ✗ | - | 90.1 | 87.6 |
| VPN [16] | ✓ | 3D | - | 93.5 | - |
| VPN++ [17] | ✓ | 3D | - | 93.5 | - |
| MMNet | ✓ | 3D | - | 93.7 | 88.7 |
| Video Swin [41] | ✓ | ✗ | 90.7 | 89.6 | 84.3 |
| MotionFormer [45] | ✓ | ✗ | 90.2 | 89.4 | 88.4 |
| TimeSformer [6] | ✓ | ✗ | 90.7 | 91.8 | 90.5 |
| PAAB (ours) | ✓ | 2D | 93.4 | 92.9 | 91.3 |
| PAAT (ours) | ✓ | ✗ | 95.4 | 92.7 | 90.8 |

and NUCLA datasets. This is despite the popularity of pure-pose based methods in these datasets, as they are more representative to our evaluation scenario. The superior performance of our models, exhaustively evaluated on cross-view protocols, underlines the *view-agnostic representation* learned by PAAB and PAAT through the use of 2D poses. Interestingly, despite solely relying on RGB, our models exhibit competitive results when compared with methods employing both RGB and 3D poses. This shows the capability of video transformers with PAAB or PAAT to capture *pose-aware features*. In addition, our models are compared with prominent video transformer models [41, 45, 6]. We find that either PAAB or PAAT, when employed with TimeSformer, surpasses the performance of state-of-the-art video transformers (except on CVS1 of NTU), boasting an absolute margin of up to 18.3%.

Multi-view robotic video alignment. Table 5 illustrates the performance of our models on the Pick, MC, Can, and Lift datasets. We present the alignment error (lower is better) for each method. Note that PAAB and PAAT are implemented in the DeiT encoder [64] which is trained with TCN losses [52]. We find that both PAAB and PAAT improves the baseline DeiT [64] by 21.8% on the MC dataset, which is notable as it contains the largest viewpoint variation of all the datasets. While our models deliver superior results compared to most of the SOTA methods, they fall slightly short of 3DTRL [55] on the Pick dataset.

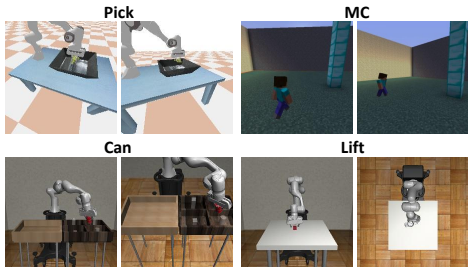


Figure 6: Example video alignment frames from two different viewpoints.

Table 5: DeiT + TCN + our pose-aware methods on multi-view robotic video alignment. Metric is alignment error.

| Method | Backbone | Pick | MC | Can | Lift |
|------------------|----------|--------------|--------------|--------------|--------------|
| TCN [52] | CNN | 0.273 | 0.286 | - | - |
| Disentangle [54] | CNN | 0.155 | 0.233 | - | - |
| 3D TRL [55] | ViT | 0.116 | 0.202 | 0.060 | 0.081 |
| DeiT [64]+TCN | ViT | 0.216 | 0.292 | 0.065 | 0.095 |
| PAAB (ours) | ViT | 0.165 | 0.151 | 0.053 | 0.075 |
| PAAT (ours) | ViT | 0.159 | 0.149 | 0.059 | 0.074 |

Video retrieval. We demonstrate the generalizability of our models, by presenting the performance of our NTU pre-trained models for video retrieval on NUCLA, as illustrated in Figure 5. However, PAAB’s performance falls short in this context, while PAAT outperforms all. This shows the generalizability power of PAAT, attributed to its joint optimization strategy.

4.6 Feature & Attention Analysis

In this section, we explore the feature space and attention distributions learned by our models on a subset of the Smarthome. In Figure 7a, we compute the average feature distance between the pose and non pose tokens in the feature space. Both PAAB and PAAT learn to better disentangle the pose and the non pose token representation compared to the baseline TimeSformer, with PAAT achieving superior feature separability due to its keypoint-specific prediction task. Figure 7b further confirms this, where PAAT exhibits better separability of individual pose features, unlike PAAB. In addition to analyzing the feature space, we also explore the attention distributions learned by our methods. In Figure 7c we report the percentage of tokens across various attention value bins at different layers.

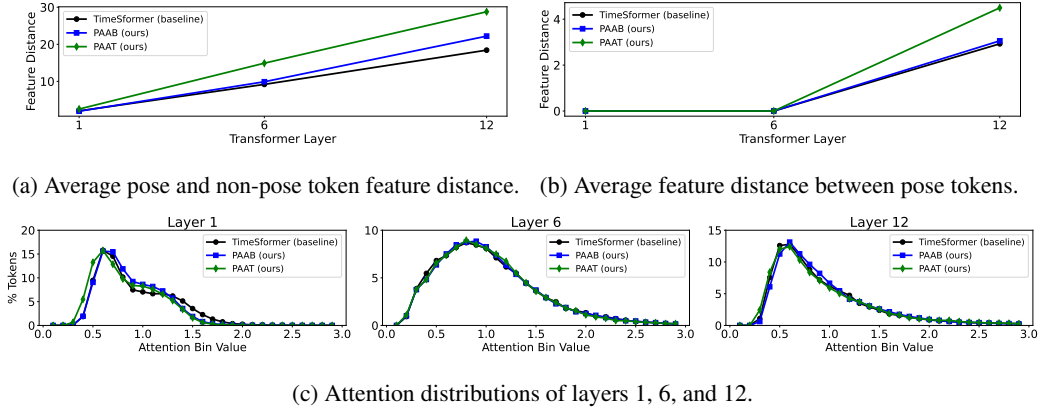


Figure 7: **Feature & Attention Analysis.** From (a) we see our methods learn to disentangle pose and non-pose tokens in the feature space. (b) shows that PAAT learns more separable pose tokens. (c) shows that interestingly, our methods maintain similar attention distributions to the baseline.

Interestingly, the attention distributions of our models align closely with the baseline, implying that our methods primarily leverage the feed-forward layers to learn pose-aware representations.

5 Related Works

In recent years, vision transformers [18, 40, 64, 73, 29, 12] have overtaken CNNs [31, 11, 63] in performance across numerous image-based tasks [18, 9, 61]. Similarly, video transformers [6, 41, 3, 45, 20, 36] have had a comparable effect on 3DCNNs [22, 37, 10, 65] and two-stream CNNs for video-based tasks [59, 23, 24]. While these video transformers are tailored for analyzing web-based videos [32, 60, 35, 27], emphasizing prominent motion patterns and frame-centric actions, they often fall short when dealing with real-world videos. These videos [68, 62, 34, 38, 53, 15, 2, 58], typically recorded in indoor settings and encompassing Activities of Daily Living (ADL), present challenges that these transformers are not designed to handle. The challenges of ADL typically includes subtle motion, videos captured from multiple camera viewpoints, and actions with similar appearance. To address these challenges of ADL, studies [71, 56, 13, 28] have been conducted on pure-pose based approaches that utilizes 2D and 3D poses. These approaches are effective on datasets recorded in laboratory settings [53, 38, 69] where human actions are not spontaneous. However, they struggle with real-world videos [17, 15] that necessitate appearance modeling of the scene to incorporate object encoding. In response, various approaches [15–17, 4, 5] have integrated RGB and pose modalities to model ADL. Notably, these methods typically utilize 3D poses, which are dependent on depth sensors or computationally intensive RGB algorithms [48, 46]. In contrast, our methods, PAAB and PAAT, leverage 2D poses, which are generally accurate and easier to obtain. The closest to our work [74, 43] perform multi-tasking for pose estimation and action recognition by sharing a 3D CNN encoder with multiple heads. Unlike these, PAAT’s multitasking (*patch-keypoint prediction task*) is tailored for use in ViTs and intriguingly, it exhibits higher effectiveness at the initial layers rather than the final layers. To our knowledge, this is the first attempt to learn a pose-aware representation using vision transformers.

6 Conclusion

In conclusion, we proposed **PAAB** and **PAAT**, two methods for learning pose-aware representations with ViTs in the first attempt at combining the RGB and 2D pose modalities into a single-stream ViT. Based on our extensive experimental analysis, we find that incorporating pose information leads to generalized ViTs that are effective across multiple tasks, and even across datasets. Surprisingly, we observe that our methods do not significantly alter the attention distributions of the backbone ViTs, and instead rely on the feed-forward layers of the model to learn pose-aware representations.

As for which method to use, *we recommend end users to prefer PAAT over PAAB* due to its consistent superior performance, enhanced generalizability and its ability to learn more fine-grained pose representations. PAAT also demands less computational resources than PAAB during inference,

necessitating no poses and additional computational parameters. However, PAAB can be a viable choice under conditions of poor pose quality and absence of computational constraints.

Future research will investigate the utilization of other entity-specific priors, like segmentation masks, to address a broad range of vision tasks.

Acknowledgments

We thank the lab members of ML Lab at UNC Charlotte for valuable discussion. We thank Jinghuan Shang and Saarthak Kapse for their helpful feedback. This work is supported by the National Science Foundation (IIS-2245652).

References

- [1] Samira Abnar and Willem Zuidema. Quantifying attention flow in transformers. In *Proceedings of the 58th Annual Meeting of the Association for Computational Linguistics*, pages 4190–4197, Online, July 2020. Association for Computational Linguistics. doi: 10.18653/v1/2020.acl-main.385. URL <https://aclanthology.org/2020.acl-main.385>.
- [2] S. Mohsen Amiri, Mahsa T. Pourazad, Panos Nasiopoulos, and Victor C.M. Leung. Non-intrusive human activity monitoring in a smart home environment. In *2013 IEEE 15th International Conference on e-Health Networking, Applications and Services (Healthcom 2013)*, pages 606–610, 2013. doi: 10.1109/HealthCom.2013.6720748.
- [3] Anurag Arnab, Mostafa Dehghani, Georg Heigold, Chen Sun, Mario Lučić, and Cordelia Schmid. Vivit: A video vision transformer. In *Proceedings of the IEEE/CVF International Conference on Computer Vision (ICCV)*, pages 6836–6846, October 2021.
- [4] Fabien Baradel, Christian Wolf, and Julien Mille. Human action recognition: Pose-based attention draws focus to hands. In *2017 IEEE International Conference on Computer Vision Workshops (ICCVW)*, pages 604–613, Oct 2017. doi: 10.1109/ICCVW.2017.77.
- [5] Fabien Baradel, Christian Wolf, Julien Mille, and Graham W. Taylor. Glimpse clouds: Human activity recognition from unstructured feature points. In *The IEEE Conference on Computer Vision and Pattern Recognition (CVPR)*, June 2018.
- [6] Gedas Bertasius, Heng Wang, and Lorenzo Torresani. Is space-time attention all you need for video understanding? In *Proceedings of the International Conference on Machine Learning (ICML)*, July 2021.
- [7] Fabian Caba Heilbron, Victor Escorcia, Bernard Ghanem, and Juan Carlos Niebles. Activitynet: A large-scale video benchmark for human activity understanding. In *Proceedings of the IEEE Conference on Computer Vision and Pattern Recognition*, pages 961–970, 2015.
- [8] Zhe Cao, Gines Hidalgo Martinez, Tomas Simon, Shih-En Wei, and Yaser Sheikh. Openpose: Realtime multi-person 2d pose estimation using part affinity fields. *IEEE Transactions on Pattern Analysis and Machine Intelligence*, 2019.
- [9] Nicolas Carion, Francisco Massa, Gabriel Synnaeve, Nicolas Usunier, Alexander Kirillov, and Sergey Zagoruyko. End-to-end object detection with transformers, 2020.
- [10] Joao Carreira and Andrew Zisserman. Quo vadis, action recognition? a new model and the kinetics dataset. In *Proceedings of the IEEE/CVF Conference on Computer Vision and Pattern Recognition (CVPR)*, pages 4724–4733. IEEE, 2017.
- [11] Ken Chatfield, Karen Simonyan, Andrea Vedaldi, and Andrew Zisserman. Return of the devil in the details: Delving deep into convolutional nets. In *The British Machine Vision Conference (BMVC)*, 2014.
- [12] Chun-Fu Richard Chen et al. Crossvit: Cross-attention multi-scale vision transformer for image classification. In *Proceedings of the International Conference on Computer Vision (ICCV)*, 2021.

- [13] Hyung-Gun Chi, Myoung Hoon Ha, Seunggeun Chi, Sang Wan Lee, Qixing Huang, and Karthik Ramani. Infogcn: Representation learning for human skeleton-based action recognition. In *2022 IEEE/CVF Conference on Computer Vision and Pattern Recognition (CVPR)*, pages 20154–20164, 2022. doi: 10.1109/CVPR52688.2022.01955.
- [14] Erwin Coumans and Yunfei Bai. Pybullet, a python module for physics simulation for games, robotics and machine learning. <http://pybullet.org>, 2016–2019.
- [15] Srijan Das, Rui Dai, Michal Koperski, Luca Minciullo, Lorenzo Garattoni, Francois Bremond, and Gianpiero Francesca. Toyota smarthome: Real-world activities of daily living. In *Proceedings of the International Conference on Computer Vision (ICCV)*, 2019.
- [16] Srijan Das, Saurav Sharma, Rui Dai, Francois Bremond, and Monique Thonnat. Vpn: Learning video-pose embedding for activities of daily living. In *European Conference on Computer Vision*, pages 72–90. Springer, 2020.
- [17] Srijan Das, Rui Dai, Di Yang, and Francois Bremond. Vpn++: Rethinking video-pose embeddings for understanding activities of daily living. *IEEE Transactions on Pattern Analysis and Machine Intelligence*, pages 1–1, 2021. doi: 10.1109/TPAMI.2021.3127885.
- [18] Alexey Dosovitskiy, Lucas Beyer, Alexander Kolesnikov, Dirk Weissenborn, Xiaohua Zhai, Thomas Unterthiner, Mostafa Dehghani, Matthias Minderer, Georg Heigold, Sylvain Gelly, Jakob Uszkoreit, and Neil Houlsby. An image is worth 16x16 words: Transformers for image recognition at scale. *Proceedings of the International Conference on Learning Representations (ICLR)*, 2021.
- [19] Yong Du, Yun Fu, and Liang Wang. Skeleton based action recognition with convolutional neural network. In *2015 3rd IAPR Asian Conference on Pattern Recognition (ACPR)*, pages 579–583, 2015. doi: 10.1109/ACPR.2015.7486569.
- [20] Haoqi Fan, Bo Xiong, Karttikeya Mangalam, Yanghao Li, Zhicheng Yan, Jitendra Malik, and Christoph Feichtenhofer. Multiscale vision transformers. In *ICCV*, 2021.
- [21] Haoshu Fang, Shuqin Xie, Yu-Wing Tai, and Cewu Lu. Rmpe: Regional multi-person pose estimation. *2017 IEEE International Conference on Computer Vision (ICCV)*, pages 2353–2362, 2016.
- [22] Christoph Feichtenhofer. X3D: expanding architectures for efficient video recognition. In *2020 IEEE/CVF Conference on Computer Vision and Pattern Recognition, CVPR 2020, Seattle, WA, USA, June 13-19, 2020*, pages 200–210. Computer Vision Foundation / IEEE, 2020. doi: 10.1109/CVPR42600.2020.00028. URL https://openaccess.thecvf.com/content_CVPR_2020/html/Feichtenhofer_X3D_Expanding_Architectures_for_Efficient_Video_Recognition_CVPR_2020_paper.html.
- [23] Christoph Feichtenhofer, Axel Pinz, and Andrew Zisserman. Convolutional two-stream network fusion for video action recognition. In *Computer Vision and Pattern Recognition (CVPR), 2016 IEEE Conference on*, pages 1933–1941. IEEE, 2016.
- [24] Christoph Feichtenhofer, Haoqi Fan, Jitendra Malik, and Kaiming He. Slowfast networks for video recognition. *CoRR*, abs/1812.03982, 2018. URL <http://arxiv.org/abs/1812.03982>.
- [25] Pallabi Ghosh, Yi Yao, Larry S Davis, and Ajay Divakaran. Stacked spatio-temporal graph convolutional networks for action segmentation. *arXiv preprint arXiv:1811.10575*, 2018.
- [26] Raghav Goyal, Samira Ebrahimi Kahou, Vincent Michalski, Joanna Materzynska, Susanne Westphal, Heuna Kim, Valentin Haenel, Ingo Fründ, Peter Yianilos, Moritz Mueller-Freitag, Florian Hoppe, Christian Thureau, Ingo Bax, and Roland Memisevic. The "something something" video database for learning and evaluating visual common sense. *CoRR*, abs/1706.04261, 2017. URL <http://arxiv.org/abs/1706.04261>.

- [27] Chunhui Gu, Chen Sun, David A. Ross, Carl Vondrick, Caroline Pantofaru, Yeqing Li, Sudheendra Vijayanarasimhan, George Toderici, Susanna Ricco, Rahul Sukthankar, Cordelia Schmid, and Jitendra Malik. AVA: A Video Dataset of Spatio-temporally Localized Atomic Visual Actions. *Conference on Computer Vision and Pattern Recognition(CVPR)*, 2018.
- [28] Ryo Hachiuma, Fumiaki Sato, and Taiki Sekii. Unified keypoint-based action recognition framework via structured keypoint pooling. *arXiv preprint arXiv:2303.15270*, 2023.
- [29] Kai Han, An Xiao, Enhua Wu, Jianyuan Guo, Chunjing Xu, and Yunhe Wang. Transformer in transformer. In A. Beygelzimer, Y. Dauphin, P. Liang, and J. Wortman Vaughan, editors, *Advances in Neural Information Processing Systems*, 2021. URL <https://openreview.net/forum?id=iF0DavhthGZ>.
- [30] Kensho Hara, Hirokatsu Kataoka, and Yutaka Satoh. Can spatiotemporal 3d cnns retrace the history of 2d cnns and imagenet? In *Proceedings of the IEEE conference on Computer Vision and Pattern Recognition*, pages 6546–6555, 2018.
- [31] Kaiming He, Xiangyu Zhang, Shaoqing Ren, and Jian Sun. Deep residual learning for image recognition. In *Proceedings of the IEEE conference on computer vision and pattern recognition*, pages 770–778, 2016.
- [32] Will Kay, Joao Carreira, Karen Simonyan, Brian Zhang, Chloe Hillier, Sudheendra Vijayanarasimhan, Fabio Viola, Tim Green, Trevor Back, Paul Natsev, et al. The kinetics human action video dataset. *arXiv preprint arXiv:1705.06950*, 2017.
- [33] Qihong Ke, Mohammed Bennamoun, Senjian An, Ferdous Ahmed Sohel, and Farid Boussaïd. A new representation of skeleton sequences for 3d action recognition. In *2017 IEEE Conference on Computer Vision and Pattern Recognition, CVPR 2017, Honolulu, HI, USA, July 21-26, 2017*, pages 4570–4579. IEEE Computer Society, 2017. doi: 10.1109/CVPR.2017.486. URL <https://doi.org/10.1109/CVPR.2017.486>.
- [34] Hema Swetha Koppula, Rudhir Gupta, and Ashutosh Saxena. Learning human activities and object affordances from rgb-d videos. In *IJRR*, 2013.
- [35] Hildegard Kuehne, Hueihan Jhuang, Estíbaliz Garrote, Tomaso Poggio, and Thomas Serre. HMDB: a large video database for human motion recognition. In *2011 International Conference on Computer Vision*, pages 2556–2563. IEEE, 2011.
- [36] Yanghao Li, Chao-Yuan Wu, Haoqi Fan, Karttikeya Mangalam, Bo Xiong, Jitendra Malik, and Christoph Feichtenhofer. Mvitv2: Improved multiscale vision transformers for classification and detection. In *CVPR*, 2022.
- [37] Ji Lin, Chuang Gan, and Song Han. Tsm: Temporal shift module for efficient video understanding. In *Proceedings of the IEEE International Conference on Computer Vision*, 2019.
- [38] Jun Liu, Amir Shahroudy, Mauricio Perez, Gang Wang, Ling-Yu Duan, and Alex C. Kot. Ntu rgb+d 120: A large-scale benchmark for 3d human activity understanding. *IEEE Transactions on Pattern Analysis and Machine Intelligence*, 2019. doi: 10.1109/TPAMI.2019.2916873.
- [39] Mengyuan Liu, Hong Liu, and Chen Chen. Enhanced skeleton visualization for view invariant human action recognition. *Pattern Recognition*, 68:346 – 362, 2017. ISSN 0031-3203. doi: <https://doi.org/10.1016/j.patcog.2017.02.030>. URL <http://www.sciencedirect.com/science/article/pii/S0031320317300936>.
- [40] Ze Liu, Yutong Lin, Yue Cao, Han Hu, Yixuan Wei, Zheng Zhang, Stephen Lin, and Baining Guo. Swin transformer: Hierarchical vision transformer using shifted windows. In *Proceedings of the International Conference on Computer Vision (ICCV)*, 2021.
- [41] Ze Liu, Jia Ning, Yue Cao, Yixuan Wei, Zheng Zhang, Stephen Lin, and Han Hu. Video swin transformer. *2022 IEEE/CVF Conference on Computer Vision and Pattern Recognition (CVPR)*, pages 3192–3201, 2021.

- [42] Ziyu Liu, Hongwen Zhang, Zhenghao Chen, Zhiyong Wang, and Wanli Ouyang. Disentangling and unifying graph convolutions for skeleton-based action recognition. In *Proceedings of the IEEE/CVF Conference on Computer Vision and Pattern Recognition*, pages 143–152, 2020.
- [43] Diogo C Luvizon, David Picard, and Hedi Tabia. 2d/3d pose estimation and action recognition using multitask deep learning. In *Proceedings of the IEEE conference on computer vision and pattern recognition*, pages 5137–5146, 2018.
- [44] Ajay Mandlekar, Danfei Xu, Josiah Wong, Soroush Nasiriany, Chen Wang, Rohun Kulkarni, Li Fei-Fei, Silvio Savarese, Yuke Zhu, and Roberto Martín-Martín. What matters in learning from offline human demonstrations for robot manipulation. In *arXiv preprint arXiv:2108.03298*, 2021.
- [45] Mandela Patrick, Dylan Campbell, Yuki M. Asano, Ishan Misra, Florian Metze, Christoph Feichtenhofer, Andrea Vedaldi, and João F. Henriques. Keeping your eye on the ball: Trajectory attention in video transformers. In Marc’Aurelio Ranzato, Alina Beygelzimer, Yann N. Dauphin, Percy Liang, and Jennifer Wortman Vaughan, editors, *Advances in Neural Information Processing Systems 34: Annual Conference on Neural Information Processing Systems 2021, NeurIPS 2021, December 6-14, 2021, virtual*, pages 12493–12506, 2021. URL <https://proceedings.neurips.cc/paper/2021/hash/67f7fb873eaf29526a11a9b7ac33bfac-Abstract.html>.
- [46] Dario Pavllo, Christoph Feichtenhofer, David Grangier, and Michael Auli. 3d human pose estimation in video with temporal convolutions and semi-supervised training. In *Conference on Computer Vision and Pattern Recognition (CVPR)*, 2019.
- [47] Shaoqing Ren, Kaiming He, Ross Girshick, and Jian Sun. Faster r-cnn: Towards real-time object detection with region proposal networks, 2016.
- [48] Grégory Rogez, Philippe Weinzaepfel, and Cordelia Schmid. LCR-Net++: Multi-person 2D and 3D Pose Detection in Natural Images. *IEEE Transactions on Pattern Analysis and Machine Intelligence*, 2019.
- [49] Michael S. Ryoo, AJ Piergiovanni, Juhana Kangasputa, and Anelia Angelova. Assemblenet++: Assembling modality representations via attention connections. In *Proceedings of the European Conference on Computer Vision (ECCV)*, 2020.
- [50] Javier Selva, Anders S. Johansen, Sergio Escalera, Kamal Nasrollahi, Thomas Baltzer Moeslund, and Albert Clap’es. Video transformers: A survey. *IEEE transactions on pattern analysis and machine intelligence*, PP, 2022.
- [51] Pierre Sermanet, Corey Lynch, Jasmine Hsu, and Sergey Levine. Time-contrastive networks: Self-supervised learning from multi-view observation. In *2017 IEEE Conference on Computer Vision and Pattern Recognition Workshops (CVPRW)*, pages 486–487, 2017. doi: 10.1109/CVPRW.2017.69.
- [52] Pierre Sermanet, Corey Lynch, Yevgen Chebotar, Jasmine Hsu, Eric Jang, Stefan Schaal, Sergey Levine, and Google Brain. Time-contrastive networks: Self-supervised learning from video. In *IEEE International Conference on Robotics and Automation (ICRA)*, pages 1134–1141. IEEE, 2018.
- [53] Amir Shahroudy, Jun Liu, Tian-Tsong Ng, and Gang Wang. Ntu rgb+d: A large scale dataset for 3d human activity analysis. In *Proceedings of the IEEE/CVF Conference on Computer Vision and Pattern Recognition (CVPR)*, June 2016.
- [54] Jinghuan Shang and Michael S. Ryoo. Self-supervised disentangled representation learning for third-person imitation learning. In *IEEE/RSJ International Conference on Intelligent Robots and Systems (IROS)*, pages 214–221, 2021. doi: 10.1109/IROS51168.2021.9636363.
- [55] Jinghuan Shang, Srijan Das, and Michael S Ryoo. Learning viewpoint-agnostic visual representations by recovering tokens in 3d space. In *Advances in Neural Information Processing Systems*, 2022.

- [56] Lei Shi, Yifan Zhang, Jian Cheng, and Hanqing Lu. Skeleton-based action recognition with multi-stream adaptive graph convolutional networks. *IEEE Transactions on Image Processing*, 29:9532–9545, 2020.
- [57] Jamie Shotton, Andrew Fitzgibbon, Mat Cook, Toby Sharp, Mark Finocchio, Richard Moore, Alex Kipman, and Andrew Blake. Real-time human pose recognition in parts from single depth images. In *CVPR 2011*, pages 1297–1304, 2011. doi: 10.1109/CVPR.2011.5995316.
- [58] Gunnar A. Sigurdsson, Gül Varol, Xiaolong Wang, Ali Farhadi, Ivan Laptev, and Abhinav Gupta. Hollywood in Homes: Crowdsourcing Data Collection for Activity Understanding. In *European Conference on Computer Vision (ECCV)*, 2016.
- [59] Karen Simonyan and Andrew Zisserman. Two-stream convolutional networks for action recognition in videos. In *Advances in neural information processing systems*, pages 568–576, 2014.
- [60] Khurram Soomro, Amir Roshan Zamir, and Mubarak Shah. UCF101: A dataset of 101 human actions classes from videos in the wild. *CoRR*, abs/1212.0402, 2012. URL <http://arxiv.org/abs/1212.0402>.
- [61] Robin Strudel, Ricardo Garcia Pinel, Ivan Laptev, and Cordelia Schmid. Segmenter: Transformer for semantic segmentation. *2021 IEEE/CVF International Conference on Computer Vision (ICCV)*, pages 7242–7252, 2021.
- [62] Jaeyongand Sung, Colin Ponce, Bart Selman, and Ashutosh Saxena. Human activity detection from rgb-d images. In *AAAI workshop*, 2011.
- [63] Christian Szegedy, Vincent Vanhoucke, Sergey Ioffe, Jon Shlens, and Zbigniew Wojna. Rethinking the inception architecture for computer vision. In *2016 IEEE Conference on Computer Vision and Pattern Recognition (CVPR)*, pages 2818–2826, 2016. doi: 10.1109/CVPR.2016.308.
- [64] Hugo Touvron, Matthieu Cord, Matthijs Douze, Francisco Massa, Alexandre Sablayrolles, and Herve Jegou. Training data-efficient image transformers: Distillation through attention. In *Proceedings of the International Conference on Machine Learning (ICML)*, volume 139, pages 10347–10357, July 2021.
- [65] Du Tran, Lubomir Bourdev, Rob Fergus, Lorenzo Torresani, and Manohar Paluri. Learning spatiotemporal features with 3d convolutional networks. In *Proceedings of the 2015 IEEE International Conference on Computer Vision (ICCV)*, ICCV ’15, pages 4489–4497, Washington, DC, USA, 2015. IEEE Computer Society. ISBN 978-1-4673-8391-2. doi: 10.1109/ICCV.2015.510. URL <http://dx.doi.org/10.1109/ICCV.2015.510>.
- [66] Gül Varol, Ivan Laptev, Cordelia Schmid, and Andrew Zisserman. Synthetic humans for action recognition from unseen viewpoints. *International Journal of Computer Vision*, 129:2264 – 2287, 2019.
- [67] Ashish Vaswani, Noam Shazeer, Niki Parmar, Jakob Uszkoreit, Llion Jones, Aidan N Gomez, Łukasz Kaiser, and Illia Polosukhin. Attention is all you need. In *Advances in neural information processing systems*, pages 5998–6008, 2017.
- [68] Jiang Wang, Zicheng Liu, Ying Wu, and Junsong Yuan. Mining Actionlet Ensemble for Action Recognition with Depth Cameras. In *IEEE International Conference on Computer Vision and Pattern Recognition (CVPR)*, 2012.
- [69] Jiang Wang, Xiaohan Nie, Yin Xia, Ying Wu, and Song-Chun Zhu. Cross-view action modeling, learning, and recognition. In *2014 IEEE Conference on Computer Vision and Pattern Recognition*, pages 2649–2656, June 2014. doi: 10.1109/CVPR.2014.339.
- [70] Saining Xie, Chen Sun, Jonathan Huang, Zhuowen Tu, and Kevin P. Murphy. Rethinking spatiotemporal feature learning: Speed-accuracy trade-offs in video classification. In *European Conference on Computer Vision*, 2017.

- [71] Sijie Yan, Yuanjun Xiong, and Dahua Lin. Spatial temporal graph convolutional networks for skeleton-based action recognition. In *Thirty-second AAAI conference on artificial intelligence*, 2018.
- [72] Bruce Yu, Yan Liu, Xiang Zhang, Sheng-hua Zhong, and Keith Chan. Mmnet: A model-based multimodal network for human action recognition in rgb-d videos. *IEEE Transactions on Pattern Analysis and Machine Intelligence*, PP:1–1, 05 2022. doi: 10.1109/TPAMI.2022.3177813.
- [73] Li Yuan, Yunpeng Chen, Tao Wang, Weihao Yu, Yujun Shi, Zi-Hang Jiang, Francis EH Tay, Jiashi Feng, and Shuicheng Yan. Tokens-to-token vit: Training vision transformers from scratch on imagenet. In *Proceedings of the IEEE/CVF international conference on computer vision*, pages 558–567, 2021.
- [74] Mohammadreza Zolfaghari, Gabriel L Oliveira, Nima Sedaghat, and Thomas Brox. Chained multi-stream networks exploiting pose, motion, and appearance for action classification and detection. In *Computer Vision (ICCV), 2017 IEEE International Conference on*, pages 2923–2932. IEEE, 2017.

Appendix

A Datasets and Protocol description

Action recognition For the task of action recognition we evaluate our methods on three popular Activities of Daily Living (ADL) datasets. **Toyota-Smarthome**[15] (Smarthome, SH) provides 16.1k video clips of elderly individuals performing actions in real-world settings. The dataset contains 18 subjects, 7 camera views, and 31 action classes. For evaluation, we follow the cross-subject (CS) and cross-view (CV1, CV2) protocols. Due to the unbalanced nature of the dataset, we use the mean class-accuracy (mCA) performance metric. The dataset provides 2D skeletons containing 13 keypoints that were extracted using LCRNet [48], which we use to generate the pose maps for our method. **NTU-RGB+D**[53] (NTU) provides 56.8k video clips of subjects performing actions in a laboratory setting. The dataset consists of 40 subjects, 3 camera views, and 60 action classes. For evaluation, we follow the cross-view-subject (CVS) protocols proposed in [66] and evaluate performance with top-1 classification accuracy. In the CVS protocols, only the 0° view from the CS training split is used for training, while testing is carried out on the 0° , 45° , and 90° view from the CS test split, which are referred to as CVS1, CVS2, and CVS3. We use the CVS protocols because they better represent the cross-view challenge. The dataset provides 2D skeletons containing 25 keypoints extracted using Randomized Decision Forest [57], which we use to generate the pose maps. **Northwestern-UCLA Multiview activity 3D Dataset**[69] (N-UCLA) contains 1200 video clips of subjects performing actions in a laboratory setting. The dataset consists of 10 subjects, 3 camera views, and 10 action classes. For evaluation, we follow the cross-view (CV) protocols in which the model is trained on two camera views and tested on the remaining view. For example, the CV3 protocol indicates the model was trained on views 1, 2 and tested on view 3. For evaluation, we report the accuracy on CV3 and the average accuracy on all cross-view protocols. We employ OpenPose [8] to extract 2D skeletons containing 18 keypoints and to generate the pose maps.

Choice of Action Recognition Datasets and protocols Contrary to popular action recognition methods evaluated on datasets like Kinetics [32] and SSV2 [26], our method targets scenarios emphasizing human poses, which we argue are crucial in Activities of Daily Living. This consideration influences our choice of datasets. Given that datasets like Kinetics often position humans centrally, close to the camera source, many poses remain obscured, thereby minimizing the relevance of skeletal data in these contexts [71].

For evaluation on NTU dataset, we follow the CVS protocols since they are challenging owing to the disparity in the training distribution. While most methodologies evaluate this dataset using Cross-subject (CS) and Cross-view (CV) protocols, these tend to be less rigorous, saturated, and do not reflect real-world scenarios. The performance of PAAB and PAAT enhance the baseline TimeSformer metrics on CS and CV protocols by a slight margin of 0.3%-0.5%, indicating that pose-aware RGB representations do not necessarily provide an additional performance boost. Nevertheless, the efficacy of the pose-aware representation, as learned from the pre-trained NTU (CS), is manifested in its generalizability for video retrieval tasks (see Fig. 5 in the main paper).

B Dataset specific Implementation details

We train all of our video models (TimeSformer based) on 8 RTX A5000 GPUs with a batch size of 32 for Smarthome and 64 for NTU and NUCLA. We train the image models (DeiT based) used in multi-view robotic video alignment on a single RTX A5000 GPU, with a batch size of 1.

Action recognition In all experiments, we follow a training pipeline similar to [6]. The RGB inputs to our models are video frames with a size of $8 \times 224 \times 224$ for Smarthome and NUCLA and a size of $16 \times 224 \times 224$ for NTU. Frames are sampled at a rate of $\frac{1}{32}$ for Smarthome and $\frac{1}{4}$ for NTU and NUCLA. To ensure that the video frames input to our model will contain pose keypoints, prior to sampling frames we first extract a 224×224 crop from the video that contains only the human subject. This can be done using the pose keypoints extracted from the RGB or by using a pre-trained human detector [47]. Our backbone model in which we insert PAAB and PAAT is a Kinetics-400 [32] pre-trained TimeSformer [6] model. For fine-tuning, we train the models for 15 epochs.

Multi-view robotic video alignment We use DeiT as a backbone architecture for inserting PAAT and PAAB and use the time-contrastive loss [51] to train our models. The training enforces that

the distance between video frames are close if the frames are temporally close, but far if they are temporally distant. We train all of our models from scratch and follow the training recipe provided in [55].

C Model Diagnosis

Figure 8: Effects of pre-training PAAB and PAAT with and without Kinetics 400 (K400) pre-training.

| Method | Pretraining | mCA |
|--------|-------------|--------------|
| PAAB | None | 71.42 |
| PAAB | K400 | 69.98 |
| PAAT | None | 72.54 |
| PAAT | K400 | 72.25 |

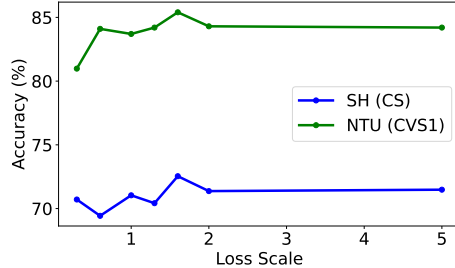


Figure 9: Ablation on the loss scale (λ) of PAAT

Varying loss scale In Figure 9 we present the results of varying PAAT’s loss scaling factor, λ . We train PAAT on the Smarthome cross-subject (SH CS) and NTU CVS1 protocols with the following values of λ : 0.3, 0.6, 1.0, 1.3, 1.6, 2.0, 5.0. We find that on both datasets, a value of $\lambda = 1.6$ is optimal for training PAAT.

Pre-training with Kinetics Surprisingly, our methods do not require Kinetics pre-training to achieve good performance. In Figure 8, we present the results of pre-training PAAB and PAAT on Kinetics-400 [32] prior to finetuning them on the Smarthome cross-subject protocol. Even more interesting is our observation that Kinetics pre-training degrades the performance of PAAB and PAAT. During Kinetics pre-training, we train the backbone without the incorporation of input poses. For PAAB, the additional block performs attention across all patches. The observed degradation in action classification performance may be attributed to discrepancies between pre-training and fine-tuning stages. This warrants the necessity of collecting more pose based real-world action recognition datasets.

FFN feature distances In Figure 10, we show that PAAB and PAAT rely on the feed-forward networks (FFNs) within the model to learn pose-aware representations. We report the average feature distance between tokens before and after the FFNs at different layers of the backbone transformer. We find that in the initial layers, both PAAB and PAAT follow a similar trend to the baseline. However around layer 6, we observe that the FFNs starts influencing the token representation. We recall that the attention distribution in PAAB and PAAT resembles with the baseline transformer. In this experiment, we find that both PAAB and PAAT alter the token representation more than the baseline, indicating that they are leveraging the FFNs rather than the attention distribution to learn pose-aware representations. This analysis reveals that the intermediate layers in transformers, particularly the

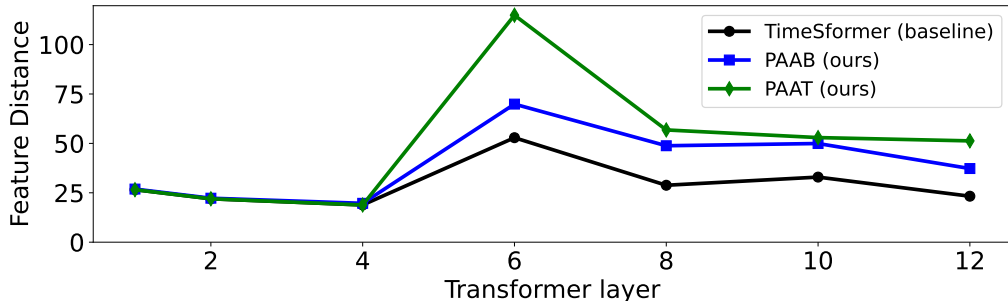


Figure 10: Average feature distance between tokens before and after the feed-forward networks.

Feed-Forward Networks (FFNs), play a pivotal role in learning pose-aware representation. However, this does not necessarily imply that PAAB and PAAT need to be integrated within these middle layers.

D Fusion of PAAB and PAAT

While we have discussed PAAB and PAAT as two different strategies for learning pose-aware video representation, we also explore their combination within a single architecture. In this experiment, we plug-in a PAAB following layer 12 of the backbone TimeSformer and invoke a keypoint-classifier based PAAT block after layer 1. Using a loss scaling factor of $\lambda = 1.6$, we observe a Smarthome (CS) action classification accuracy of 69.9%, as compared to 71.4% and 72.5% achieved by PAAB and PAAT respectively. We argue that this drop in performance is owing to the conflicting gradients generated by the introduction of both modules (PAAB & PAAT).

E Limitations

As previously mentioned, PAAB and PAAT are two distinct yet complementary methods for learning pose-aware representation, each possessing their unique strengths and weaknesses. The exploration of a strategy to integrate the benefits of both methods remains an open challenge. The amalgamation of both methods into a single model could potentially yield a more robust framework compared to individual models.

Additionally, another key limitation of PAAB and PAAT is their dependency on pose data during training. Although recent advances have facilitated pose extraction from RGB [8], the associated computational costs remain a challenge for training our methodologies. Moreover, PAAB necessitates pose information during inference, along with the inclusion of additional parameters, thereby extending the inference time.